Mechanism and Machine Theory 69 (2013) 115–126

Contents lists available at ScienceDirect

Mechanism and Machine Theory

journal homepage: www.elsevier.com/locate/mechmt

Influence of external excitations on ball positioning of an automatic balancer

C.K. Sung [a,*], T.C. Chan [a,c], C.P. Chao [b], C.H. Lu [a]

[a] Department of Power Mechanical Engineering, National Tsing Hua University, Hsinchu 30013, Taiwan, ROC
[b] Department of Electrical and Computer Engineering, National Chiao Tung University, Hsinchu 30010, Taiwan, ROC
[c] Precision Machinery Research and Development Center, Taichung 40768, Taiwan, ROC

ARTICLE INFO

Article history:
Received 18 February 2012
Received in revised form 30 April 2013
Accepted 27 May 2013
Available online 16 June 2013

Keywords:
Ball positioning
Automatic ball balancer (ABB)
External excitation

ABSTRACT

This study examined the influence of external excitations on ball positioning in an automatic ball balancer (ABB) installed in a rotor system. The authors' previous studies adopted a model that considered the ABB as an autonomous system by neglecting external excitations. We examined how the magnitude, the frequency and even the phase of an external excitation affected ball positioning. Simulations were performed to predict the ball positions under various external forces. Then, we constructed an experimental rig by employing a shaker to apply excitations to the rotor system and the associated ABB to verify the theoretical development. Simulation results indicated that the balancing balls of the ABB could counterbalance the external force by the change of the ball positions. However, it was observed from the experiment that the ball would not be displaced if the external force was applied after the ball had been positioned because the excessive rolling resistance between the ball and the runway prevented the ball from moving to desired positions.

1. Introduction

An ABB can automatically and continually counteract the unbalance in rotating machinery, so it has been employed in various machine tool systems. In practice, a large number of machine tools are installed on one floor, not necessarily the ground floor, of a factory where the machining forces and floor vibrations resulted external excitations may not be avoidable. This may drastically deteriorate the performance of the ABB because the external force causes inaccurate ball positioning.

Thearle [1] presented an early analysis of various types of balancing systems and found ball-type balancers to be superior to other types because of their low friction, low cost, and ease of implementation. Majewski [2] investigated the rolling resistance of ball motion, the eccentricity of the runway and the influence of external vibrations, which caused in accuracies in positions of the balancing bodies. Huang et al. [3] introduced a simple stick-slip model and illustrated the unavoidable rolling friction between the balancing balls and the runway flange, which actually deterred the balls from remaining precisely at the desired positions. Chao et al. [4,5] presented non-planar and torsional motions dynamic modelling and analysis to reaffirm the capability of the ABB system. Horvath et al. [6] set up an experimental investigation of ball balancer and find the rolling friction when the deformation of the contact point of the ball and channel surface by the centripetal acceleration. DeSmidt [7] explored the dynamics and stability of an unbalanced flexible shaft equipped with an ABB. An effective force ratio parameter governing the equilibrium behavior of flexible shaft and ABB was identified. Liu and Ishida [8] presented a vibration suppression method utilising the discontinuous spring characteristics together with an ABB. Ehyaei and Moghaddam [9] developed a system of unbalanced flexible rotating shafts equipped with *n*ABBs, where the unbalanced masses were distributed along the lengths of the shafts. Green et al. [10] presented a

* Corresponding author. Tel.: +886 3 5742918; fax: +886 3 5715314.
E-mail addresses: cksung@pme.nthu.edu.tw (C.K. Sung), d9533830@oz.nthu.edu.tw (T.C. Chan), pchao@mail.nctu.edu.tw (C.P. Chao), d9533827@oz.nthu.edu.tw (C.H. Lu).

0094-114X/$ – see front matter © 2013 Elsevier Ltd. All rights reserved.
http://dx.doi.org/10.1016/j.mechmachtheory.2013.05.009

Nomenclature

G_R	Centre of gravity (C.G.) of the equivalent rotor
G_S	Centre of gravity of the equivalent stator
M_R	Mass of the equivalent rotor
M_S	Mass of the equivalent stator
O_B	Centre of a ball
O_S	Rotational centre of the rotor
O_R	Origin of the inertial coordinate system
O_r	Centre of the circular runway of the balancer
e	Unbalanced eccentricity
β	Lead angle of the unbalance
ϕ_i	Angles of ball's positions
B_i	Number of balls
m	Ball mass
r	Ball radius
K_X	Stiffness in the X direction
K_Y	Stiffness in the Y direction
C_X	Damping in the X direction
C_Y	Damping in the Y direction
p	Speed ratio ω/ω_n
ε	Scaling parameter $\sqrt{m/M}$
ω_n	Natural frequency of the suspension
τ	Normalised time scale
R	Runway radius
α_1	Adhesive coefficient
α_0	Rolling friction coefficient of the ball balancer
θ	Rotating angle of the disc
F	External force
ω_e	External force frequency
ω_r	Rotational frequency
δ	Phase angle of external force
F_f	Friction force between the ball and runway flange
η	Angle corresponding to the coefficient of rolling friction
a_t	Tangential acceleration of the ball
a_n	Inertial acceleration of the ball
a_w	Runway flange acceleration
$\ddot{\alpha}_B$	Ball angular acceleration relative to runway outer flange

nonlinear bifurcation analysis of a two-ball, automatic, dynamic balancing mechanism for eccentric rotors. Rodrigues et al. [11] presented a model of a two-plane ABB that included the effects of support anisotropy and rotor acceleration. Chan et al. [12] investigated the effects of non-linear suspensions of an ABB installed in a rotor system on ball positioning. Lu and Wang [13] analysed a new design of an auto balancer that was designed to increase the stable region of perfect balancing. The effects of vibration reduction by the ABB, therefore, need to be re-evaluated with an emphasis on the influence of rolling friction. Quangang et al. [14] and Chan et al. [15] investigated the influence of friction in an ABB. De Wouw et al. [16] evaluated the performance of an ABB with dry friction. Except the use of automatic ball balancers, Horvath et al. [17] demonstrated analytically that a two-pendulum self-balance system, in conjunction with a spherical joint, could eliminate both dynamic and static imbalances in a rotating disc.

The authors' previous studies adopted a model that considered the ABB as an autonomous system by neglecting external excitations. That is, the excitation force on the rotor is resulted solely from the unbalance of the rotor system itself. We will examine how the magnitude, the frequency and even the phase of an external excitation affected ball positioning. The equations governing the motions of the rotor system and the balancing balls under external forces will be derived by the Lagrange method. Then, simulations will be performed to predict the ball positions under various external forces. Finally, an experimental rig is established by employing a shaker to apply excitations to a rotor system and the associated ABB to verify the theoretical development.

2. Mechanical modelling and governing equations

The unbalance in rotating machinery commonly produces harmonic excitation to the rotor system. Meanwhile, the rotor system may also experience external excitations to cause additional vibrations. For example, a large number of machine tools are

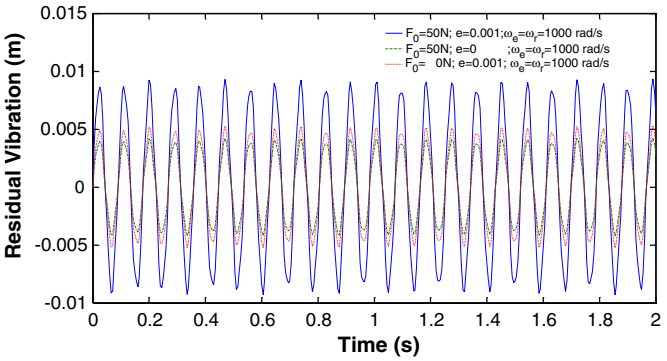

Fig. 1. Residual vibration of a rotor system due to its unbalance and an external excitation.

often installed on one floor of a factory where the machining forces and floor vibrations may create excitations upon each other. External forces can be broadly characterised as either impulse, random or harmonic excitation. For example, a single-DOF system with rotating unbalance, $me\omega_r^2 \sin \omega_r t$, is excited by an external force $F = F_0 \sin \omega_e t$ with the forcing frequency identical to the rotational frequency, i.e., $\omega_e = \omega_r$. As the system is not installed with automatic ball balancer (ABB), it can be observed in Fig. 1 that the external force does increase the amplitude of the residual vibration of the rotor system. In the following study, it is proved that the balancing balls of the ABB can counterbalance an external force by changing their positions if the ball's driving force is larger than the rolling resistance between the ball and the runway. Otherwise, the external excitation may significantly deteriorate the performance of the ABB because the balls cannot move to the desired positions.

The physical system of an ABB is simplified and illustrated schematically in Fig. 2. An equivalent model of the rotor represents the rotating parts of the system containing the disc and the rotor of the spindle motor. The non-rotating parts constitute an equivalent stator that contains the foundational structure and the stator of the spindle motor, and its driving unit. The rotor shaft is treated as a rigid body, and the stator of the spindle motor, its foundation, and drive unit is also considered as rigid bodies.

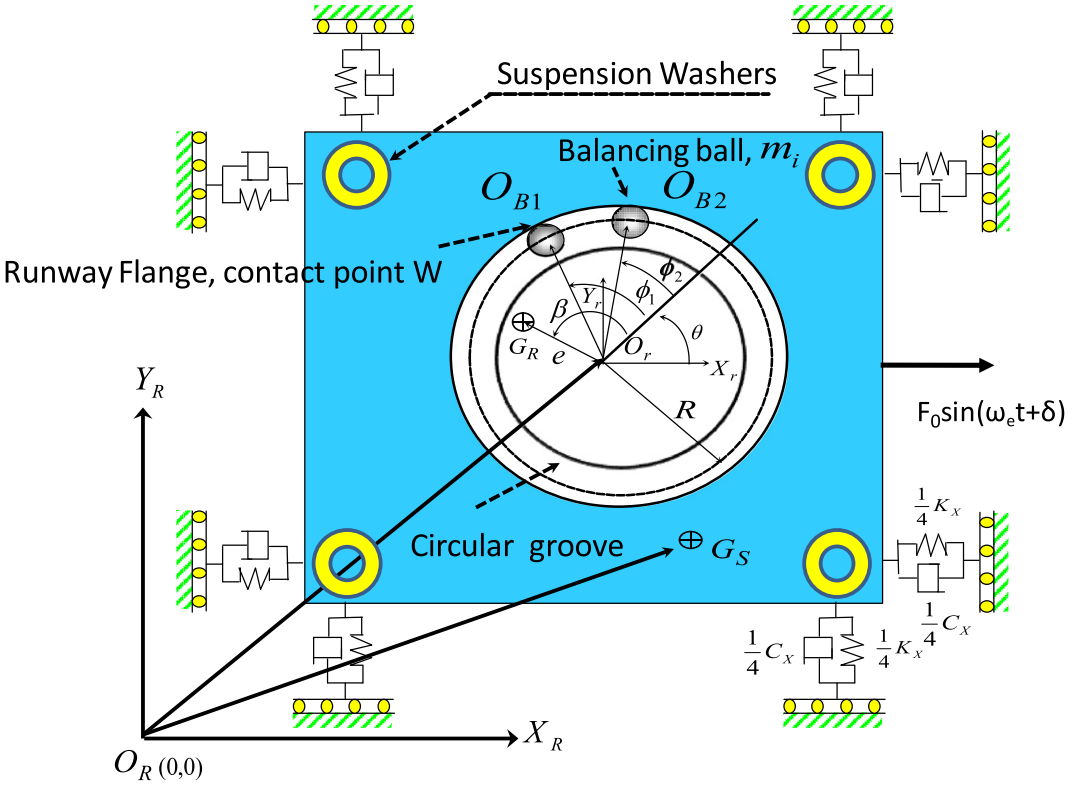

Fig. 2. Mechanical model of the rotor system.

The motion of the unbalanced rotor is mainly in the radial direction because of the horizontal flexibility of the damping washers that constitute the suspension system. The flexibility of these washers is assumed to be characterised by equivalent linear springs and dampers, denoted by (K_X,K_Y) and (C_X,C_Y), respectively. With the following assumptions for the stator–rotor-foundation system, the radial vibrations are reduced by ball balancers.

The shape of the balancer's runway is a perfect circle and the balls are assumed to be perfect spheres. While the balls, considered as point masses, move along the runway, they always keep point contacts with the outer flange of the runway, which is true during actual operation at the steady state because of the centrifugal force. The gravitational effect on the balls is small compared to the centrifugal field. No slip occurs while the balls move because the slip friction is much greater than the rotational friction. The following analysis is based on the physical system in Fig. 2, where, without a loss of generality, only two balls with mass m and radius r are illustrated. G_R and G_S denote the centres of gravity (C.G.s) of the equivalent rotor and stator, respectively, M_R and M_S are the corresponding masses, O_{B1} and O_{B2} denote the centres of the balls, and O_R denotes the origin of the inertial coordinate system $O_RX_RY_R$. O_r denotes the centre of the balancer's circular runway, and the origin of the moving coordinate system is $O_rX_rY_r$. The C.G. eccentricity of the equivalent rotor relative to O_r is represented by e; i.e., $e = |\overrightarrow{O_rG_R}|$. The angle θ, defined in coordinate system $O_rX_rY_r$, denotes the rotation angle of the disc. The angle β, defined in coordinate system $O_rX_rY_r$, denotes the lead angle of the rotor's C.G. location with respect to the current angular position of the rotor. The angles ϕ_1 and ϕ_2, defined in coordinate system $O_rX_rY_r$, denote the lead angles of the balls' positions with respect to the current angular position of the rotor.

2.1. Kinetic energy

Using the notation defined, the kinetic energy can be obtained as follows. Let

$$\overrightarrow{O_RG_R} = \begin{bmatrix} X \\ Y \end{bmatrix} + e\begin{bmatrix} \cos(\beta+\theta) \\ \sin(\beta+\theta) \end{bmatrix} \tag{1}$$

$$\overrightarrow{O_RO_B} = \begin{bmatrix} X \\ Y \end{bmatrix} + R\begin{bmatrix} \cos(\phi+\theta) \\ \sin(\phi+\theta) \end{bmatrix} \tag{2}$$

$$\overrightarrow{O_RO_r} = \begin{bmatrix} X \\ Y \end{bmatrix} \tag{3}$$

$$\overrightarrow{O_RO_W} = \begin{bmatrix} X \\ Y \end{bmatrix} + (R+r)\begin{bmatrix} \cos(\phi+\theta) \\ \sin(\phi+\theta) \end{bmatrix}, \tag{4}$$

where $\overrightarrow{O_RG_R}$, $\overrightarrow{O_RO_B}$, $\overrightarrow{O_RO_r}$, and $\overrightarrow{O_RO_W}$ represent the displacement vectors of the equivalent stator, the two balls, the rotor, and the runway flange for the balancing ball, respectively. The kinetic energy of the system is contained in the equivalent stator, the balls, the rotor and the runway. Herein, the moment of inertia of the ball is considered. According to the assumptions of no slip between the ball and the runway and the perpendicularity of the ball's spinning axis to the ABB circular bottom plane, the angular velocity of the ball spin is $\dot{\alpha}_B$, where $\dot{\alpha}_B = \left|\dot{\overrightarrow{O_RO_W}} - \dot{\overrightarrow{O_RO_B}}\,/r\right|$. The rotational energy of the ball is

$$T_{Br} = \frac{1}{2}I_B\dot{\alpha}_B{}^2 = \frac{1}{2}\frac{I_B}{r^2}\left|\dot{\overrightarrow{O_RO_W}} - \dot{\overrightarrow{O_RO_B}}\right|^2, \tag{5}$$

where I_B and r are the moment of inertia and radius of the balancing ball, respectively. Based on Eqs. (1)–(5), the total kinetic energy can be obtained as

$$T = T_s + T_R + 2(T_B + T_{Br}) = \frac{1}{2}M_S\left|\dot{\overrightarrow{O_RG_R}}\right|^2 + \frac{1}{2}M_R\left|\dot{\overrightarrow{O_RO_r}}\right|^2 + m_i\left|\dot{\overrightarrow{O_RO_B}}\right|^2 + \frac{I_B}{r^2}\left|\dot{\overrightarrow{O_RO_W}} - \dot{\overrightarrow{O_RO_B}}\right|^2. \tag{6}$$

2.2. Potential energy

The deformation of the spring creates the potential energy V:

$$V = \frac{1}{2}K_XX^2 + \frac{1}{2}K_YY^2, \tag{7}$$

where K_X and K_Y are the stiffnesses in the X and Y directions of the washers, respectively.

2.3. Generalised forces

Assuming no slip occurs between the ball and the runway flange, the friction force, denoted by F_f, induces a rolling moment on the ball. Acting on the ball area drag force D due to the interaction between the ball motion and surrounding fluid and a rolling

resistance moment M_f, mainly, due to the rolling friction with the runway's outer flange. The interactive dynamics between the balancing and runway flange is next discussed to derive the equations of motion for balancing balls. Fig. 3(a) shows the free-body diagram of balancing ball where ball material is assumed much stiffer than the runway material which causes a small bump deformation in the frontal area of running ball. Then, defined in the inertia coordinates $O_RX_RY_R$, are next derived to capture the dynamics of the ball. As illustrated in Fig. 3(c), the net ball acceleration can be decomposed into tangential acceleration a_t and runway flange acceleration a_w. Through the transformations bridging the inertial coordinates $O_RX_RY_R$ and the translating coordinate $O_rX_rY_r$, a_t and a_w can be formulated by

$$a_t = R\left(\ddot{\phi}+\ddot{\theta}\right) - \ddot{X}\sin(\phi+\theta) + \ddot{Y}\cos(\phi+\theta) \tag{8}$$

$$a_w = (R+r)\ddot{\theta} - \ddot{X}\sin(\phi+\theta) + \ddot{Y}\cos(\phi+\theta). \tag{9}$$

Compared to the case of motionless ball, this deformation shifts the contact point between the ball and runway flange from downright position to the one with a corresponding angle, η, deviating from the downright direction. In order to construct the equations of motion of the ball that is described in the coordinates defined, the acting point of the forces in the original free-body diagram is translated to the downright position as shown in Fig. 3(b) with the generation of a moment

$$M_f = Nr\sin\eta + F_f r(1-\cos\eta) \tag{10}$$

which deters the ball rolling forward, thus named by "rolling resistance moment." In Eq. (10), η, in practice, can be assumed small, thus, $M_f \approx Nr\sin\eta$. N is the reaction force which is equivalent to the inertial force generated by the ball in the centrifugal field. $N = ma_n$, where a_n represents the inertial acceleration of the ball induced by the centrifugal field. a_n can be formulated by

$$a_n = R\left(\dot{\theta}+\dot{\phi}_i\right)^2 - \ddot{X}\cos(\theta+\phi_i) - \ddot{Y}\sin(\theta+\phi_i). \tag{11}$$

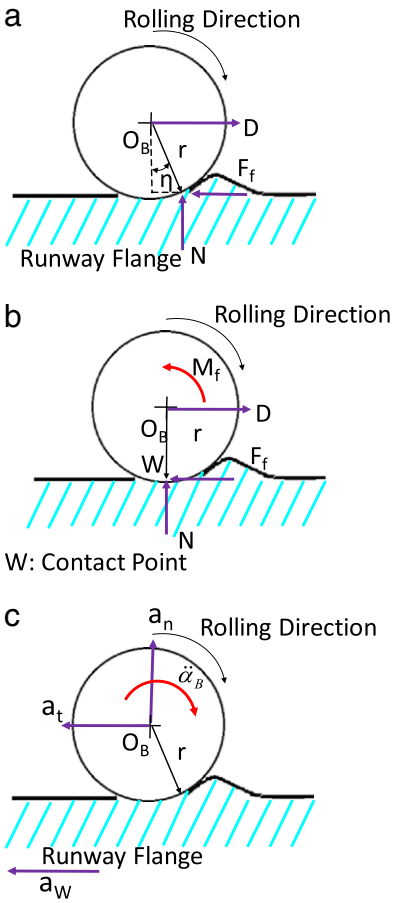

Fig. 3. Actions of forces on the ball: (a) Free-body diagram, (b) equivalent free-body diagram, and (c) accelerations.

Balancing the forces and moments acting on the ball as shown in Fig. 3(a) leads to two equilibrium equations

$$F_f - D\,\mathrm{sgn}\left(\dot{\phi}\right) = ma_t \tag{12}$$

$$F_f r - M_f\left[-\mathrm{sgn}\left(\dot{\phi}\right)\right] = I\ddot{\alpha}_B, \tag{13}$$

where $\ddot{\alpha}_B$ is the ball angular acceleration relative to runway outer flange, and the term $D\,\mathrm{sgn}\left(\dot{\phi}\right)$ represents the drag force due to the interaction between ball motion and surrounding fluid. This term can be assumed in an alternative form $\alpha_1 R\dot{\phi}$, the product of the adhesive coefficient α_1 and relative velocity of the ball to runway flange.

$F = F_0\sin(\omega_e t + \delta)$ is the external force with frequency ω_e and phase angle δ. The generalised forces due to the damping washers can be represented as $-C_X\dot{X}$ and $-C_Y\dot{Y}$ acting in the X and Y directions, respectively. Thus, the generalised forces can be derived as

$$Q_{qk} = -C_X\dot{X} - C_Y\dot{Y} - D - \frac{M_f}{r}\left(-\mathrm{sgn}\dot{\phi}\right) + F_0\sin(\omega_e t + \delta). \tag{14}$$

Herein, D is the product of the adhesive coefficient α_1 and the relative velocity of the balls to the runway flange.

$$D = \alpha_1 R\dot{\phi} \tag{15}$$

The moment M_f is obtained from

$$M_f = \alpha_0 m\left[R\left(\dot{\theta} + \dot{\phi}_i\right)^2 - \ddot{X}\cos(\theta + \phi_i) - \ddot{Y}\sin(\theta + \phi_i)\right], \tag{16}$$

where α_0 is the rolling friction coefficient of the ball, given by $\alpha_0 \equiv r\sin\eta$.

2.4. Equations of motion

Given the kinetic energy, the potential energy, and the generalised forces, the equations governing the motion of the system can be derived with Lagrange's equation

$$\frac{d}{dt}\left(\frac{\partial L}{\partial \dot{q}_k}\right) - \left(\frac{\partial L}{\partial \dot{q}_k}\right) = Q_{qk}, \tag{17}$$

where $L = T - V$, Q_{qk} is the generalised forces, and q_k is the generalised coordinates. Thus, the equations of motion for the rotor system can then be obtained as follows:

$$\begin{aligned} M\ddot{X} + C_X\dot{X} + K_X X = {} & F_0\sin(\omega_e t + \delta) + M_R\left[e\ddot{\theta}\sin(\theta + \beta) + e\dot{\theta}^2\cos(\theta + \beta)\right] \\ & + m\sum_{i=1}^{n}\left[R\left(\ddot{\theta} + \ddot{\phi}_i\right)\sin(\theta + \phi_i) + R\left(\dot{\theta} + \dot{\phi}_i\right)^2\cos(\theta + \phi_i)\right], \end{aligned} \tag{18}$$

$$\begin{aligned} M\ddot{Y} + C_Y\dot{Y} + K_Y Y = {} & M_R\left[-e\ddot{\theta}\cos(\theta + \beta) + e\dot{\theta}^2\sin(\theta + \beta)\right] \\ & + m\sum_{i=1}^{n}\left[-R\left(\ddot{\theta} + \ddot{\phi}_i\right)\cos(\theta + \phi_i) + R\left(\dot{\theta} + \dot{\phi}_i\right)^2\sin(\theta + \phi_i)\right], \end{aligned} \tag{19}$$

$$\begin{aligned} \left(m_i + \frac{I}{r^2}\right)R\left(\ddot{\phi}_i + \ddot{\theta}\right) = {} & m_i\left[\ddot{X}\sin(\phi_i + \theta) - \ddot{Y}\cos(\phi_i + \theta)\right] \\ & - \alpha_1 R\dot{\phi}_i - \frac{M_f}{r}\,\mathrm{sgn}\left(\dot{\phi}_i\right) + \frac{(R + r)}{r^2}I\ddot{\theta}, \end{aligned} \tag{20}$$

where $M = M_R + M_S + nm$, with M_R, M_S, and m denoting the masses of the equivalent rotor, the stator, and the ball, respectively, and n denotes the number of balls.

Rearranging Eq. (20) yields the equation for the driving forces applied to the balancing ball

$$\begin{aligned} \left(m_i + \frac{I}{r^2}\right)R\ddot{\phi}_i = {} & m_i\left[\ddot{X}\sin(\phi_i + \theta) - \ddot{Y}\cos(\phi_i + \theta)\right] \\ & - \alpha_1 R\dot{\phi}_i - \frac{M_f}{r}\,\mathrm{sgn}\left(\dot{\phi}_i\right) + \left(\frac{I}{r} - m_i R\right)\ddot{\theta}. \end{aligned} \tag{21}$$

Table 1
Values of system parameters.

Parameter	Symbol	Values (unit)
Natural frequency of the linear spring	ω_n	11.2 Hz
Mass of the equivalent stator	M_S	110 g
Mass of the equivalent rotor	M_R	40 g
Ball mass	m	0.14 g
Ball radius	r	1 mm
Runway radius	R	16.5 mm
Equivalent suspension damping	C_X & C_Y	$C_X = C_Y \approx 2\zeta M\omega_n$
Damping ratio	ζ	0.025
C.G. eccentricity	e	0.1 mm
Adhesive coefficient	α_1	2×10^{-5}(N × s/m^2)
Lead angle of the unbalance	B	90°
Rolling friction coefficient	α_0	0 m

Eq. (21) can be rewritten in the following form

$$\left(m_i + \frac{I}{r^2}\right)R\left(\ddot{\phi}_i\right) = F_I + F_D + F_R \tag{22}$$

where

$$F_I = \left(\frac{I}{r} - m_i R\right)\ddot{\theta}, F_D = m_i\left[\ddot{X}\sin(\phi_i + \theta) - \ddot{Y}\cos(\phi_i + \theta)\right], F_R = -\alpha_1 R\dot{\phi}_i - \frac{M_f}{r}\,\mathrm{sgn}\left(\dot{\phi}_i\right)$$

F_I, F_D and F_R are, respectively, the driving forces on the ball generated from angular acceleration of the rotor, the translational vibration of the suspension, and the rolling resistance and the viscous drag between ball and runway.

Approximate solutions are sought by assuming some scaling to manipulate the equations of motion, Eqs. (18)–(20), and by applying techniques of asymptotic multiple-scale analysis [12,15]:

$$\begin{aligned}&\varepsilon = \sqrt{n/M}, \omega_n\sqrt{K/m}, \varepsilon x = X/R, \varepsilon y = Y/R, p = \omega_r/\omega_n, \tau = \omega_n t, \varepsilon^2\lambda_2 = e/R, \varepsilon\zeta_1 = \alpha_1/m\omega_n, \mu = m/\left(m + I/r^2\right),\\ &\varepsilon\lambda = (r+R)I/mr^2R, F_{eq} = F_0/MR\omega_n^2, \varepsilon\zeta = C/M\omega_n, \varepsilon\zeta_0 = \alpha_0/r, \alpha = M_R/M,\end{aligned} \tag{23}$$

where the small parameter ε serves as a small scaling parameter, and τ is a normalised time scale. Substituting Eq. (23) into the system equations of motion, Eqs. (18)–(20) are solved for the case of two balls ($n = 2$) and a constant rotational speed near the point of linear resonance. Note that $\ddot{\theta} = 0, \dot{\theta} = p, \theta = p\tau$. To facilitate the ensuing asymptotic analysis, the square of the speed ratio p is represented by $p^2 = 1 + \varepsilon\sigma$, where σ captures the scaled deviation of p^2 from one. Note that the scaling $p^2 = 1 + \varepsilon\sigma$ implies that the analysis in this paper is only valid near the natural frequency of the system. However, because of weak excitation, no super or sub-harmonic resonance is present, as shown in the equations, the approximate solutions may be able to predict the dynamics away from the primary resonance. Substituting, we obtain

$$\ddot{x} + p^2 x = \varepsilon\begin{bmatrix}-\zeta\dot{x} + \sigma x + \alpha p^2\lambda_2\cos(p\tau + \beta) + \ddot{\phi}_1\sin(p\tau + \phi_1) + \ddot{\phi}_2\sin(p\tau + \phi_2)\\ +\left(p + \dot{\phi}_1\right)^2\cos(p\tau + \phi_1) + \left(p + \dot{\phi}_2\right)^2\cos(p\tau + \phi_2) + F_{eq}\sin(\tau\omega_r/\omega_e + \delta)\end{bmatrix}, \tag{24}$$

$$\ddot{y} + p^2 y = \varepsilon\begin{bmatrix}-\zeta\dot{y} + \sigma y + \alpha p^2\lambda_2\sin(p\tau + \beta) - \ddot{\phi}_1\sin(p\tau + \phi_1) - \ddot{\phi}_2\sin(p\tau + \phi_2)\\ +\left(p + \dot{\phi}_1\right)^2\sin(p\tau + \phi_1) + \left(p + \dot{\phi}_2\right)^2\sin(p\tau + \phi_2)\end{bmatrix}, \tag{25}$$

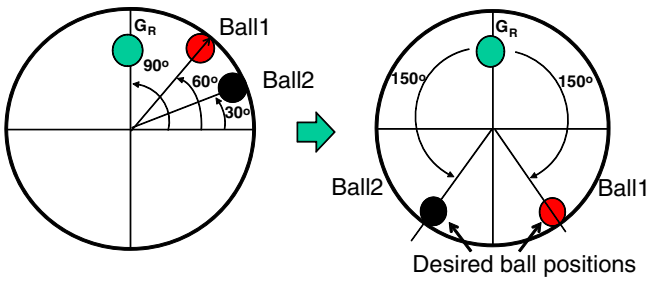

Fig. 4. Initial angles of balls and desired ball positions.

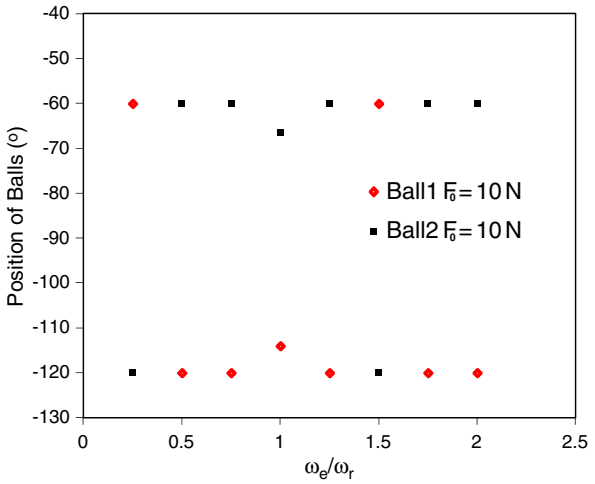

Fig. 5. Ball positions as the rotor system is under the external forces with varying frequencies.

$$\ddot{\phi}_1 = \varepsilon\mu\left\{\begin{array}{l}\ddot{x}\sin(p\tau+\phi_1)-\ddot{y}\cos(p\tau+\phi_1)-\zeta_1\dot{\phi}_1-\zeta_0\left[\left(p+\dot{\phi}_1\right)^2-\varepsilon\ddot{x}\cos(p\tau+\phi_1)\right.\\ \left.-\varepsilon(\ddot{y})\sin(p\tau+\phi_1)\right]\operatorname{sgn}\left(\dot{\phi}_1\right)\end{array}\right\}, \tag{26}$$

$$\ddot{\phi}_2 = \varepsilon\mu\left\{\begin{array}{l}\ddot{x}\sin(p\tau+\phi_2)-\ddot{y}\cos(p\tau+\phi_2)-\zeta_1\dot{\phi}_2-\zeta_0\left[\left(p+\dot{\phi}_2\right)^2-\varepsilon\ddot{x}\cos(p\tau+\phi_2)\right.\\ \left.-\varepsilon\ddot{y}\sin(p\tau+\phi_2)\right]\operatorname{sgn}\dot{\phi}_2\end{array}\right\}. \tag{27}$$

Using Eqs. (24)–(27), we could conduct the following simulations.

3. Simulations

The parameters and their corresponding values, listed in Table 1, are related to optical disc drives manufactured by Lite-On IT Corporation, Taiwan. The maximal counterbalance (two balls sticking together) has to be greater than the inherent unbalance in this case ($2mR > M_Re$).

Fig. 4 illustrates the positions of the pair of balls, which are initially at the angles 30° and 60°. The balancing balls are situated 150° opposite from the inherent unbalance, G_r, when the external forcing frequency is not equal to rotational frequency ($\omega_e \neq \omega_r$), or the magnitude of the external force $F_0 = 0$. The prefect balancing of the ball positions can be verified by the following equation:

$$2 \times m \times R \times Cos(180-150)^\circ = M_R \times e. \tag{28}$$

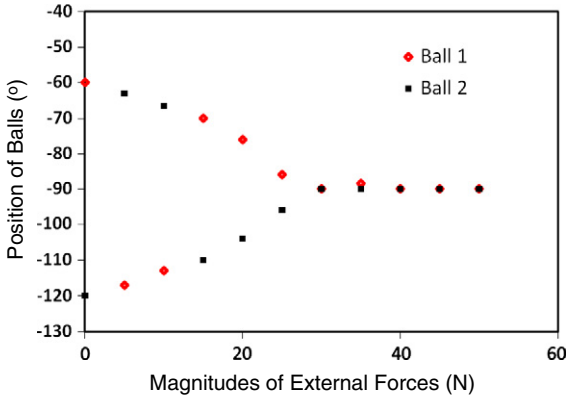

Fig. 6. Ball positions affected by the magnitudes of external forces when $\omega_r = \omega_e$.

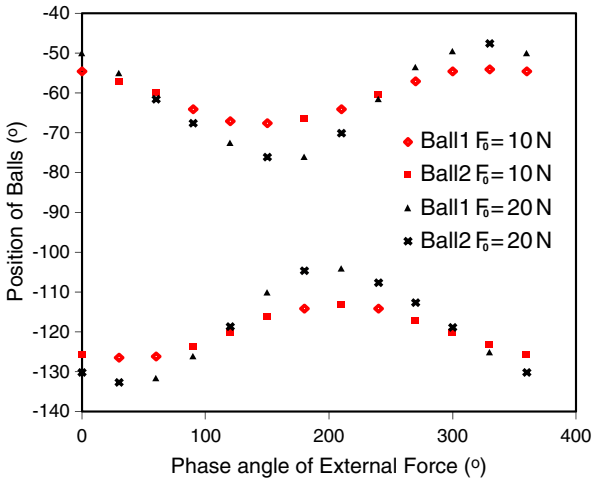

Fig. 7. Ball positions affected by both phase angles and magnitudes of external forces when $\omega_r = \omega_e$.

When an external force $F = F_0 \sin(\omega_e t + \delta)$ is applied to the rotor system in X direction with a magnitude of 10 N and a frequency equal to the rotational frequency ($\omega_e = \omega_r$), the balancing balls are situated 156° from the inherent unbalance. Thus, the ball positions are affected by the external force when its frequency is equal to the rotational frequency ($\omega_e = \omega_r$), as shown in Fig. 5.

Fig. 6 shows that the two balls come closer together until they contact with each other as the magnitude of the external force increases. It indicates that the balancing balls of the ABB can also counterbalance the external force by changing their positions. The oscillatory variation of the ball positions shown in Fig. 7 presents the effect of the phase angle of the external force when $\omega_e = \omega_r$. The ball positions are affected by both the magnitude and the phase angle of the external force when the external forcing frequency is equal to the rotational frequency; i.e., $\omega_e = \omega_r$. The two balancing balls may interchange steady-state position on the basis of the different magnitudes, the frequency and even the phase of an external excitation. The driving force of the balancing balls is also affected by the varying phase angle of the external force, as shown in Fig. 8. The variation of the ball positions can counterbalance the centrifugal force of the unbalanced mass and the external force.

4. Experimental study

An experimental study was performed to verify the derived mathematical expressions. Fig. 9 shows a photograph of the experimental apparatus which includes six subsystems: a balancer system containing two balancing balls, a spindle motor accompanied by a servo box, a shaker associated with a load cell, two accelerometers, a stroboscope and a signal analyser.

In the experiment, the spindle motor and the shaker were started up simultaneously until the rotor was accelerated to the desired speeds. We used the stroboscope to observe the steady-state angular positions of the balls. As the balls settled into their steady-state positions, the force and accelerations of the rotor were measured by the load cell and accelerometers, respectively, and were recorded by the signal analyser. Fig. 10 illustrates two external forces acting on the system: one with the forcing frequency identical to rotational one while the other not identical. The forces measured by the load cell were generated from not

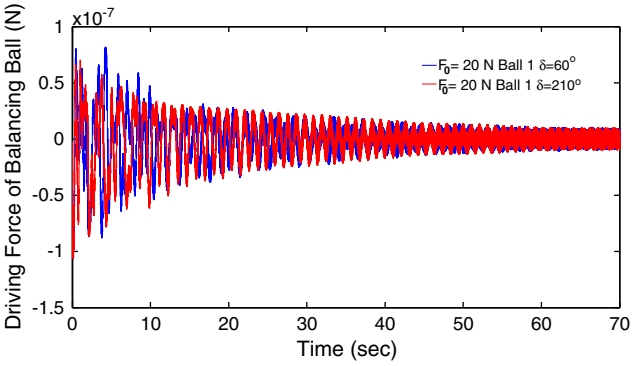

Fig. 8. The driving force of balancing balls with a varying phase angle of the external force.

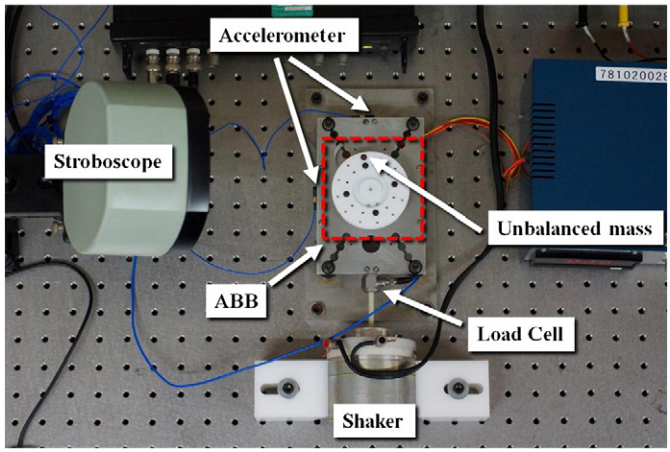

Fig. 9. Photograph of the experimental apparatus.

only the shaker but also the rotor's residual vibrations. It can be observed in Fig. 11 that the ball positions are affected by the external force when $\omega_r = \omega_e$, which are close to the theoretical predictions shown in Fig. 6 with an external force, $F_0 = 15$ N. The results verify the capability of the mathematical model constructed in the previous section.

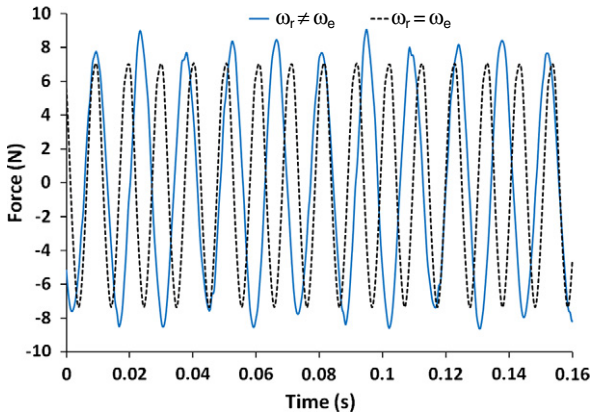

Fig. 10. Forces acting on the system with different frequencies ($\omega_r = 97$Hz, $\omega_e = 70$ Hz) and ($\omega_r = \omega_e = 97$ Hz).

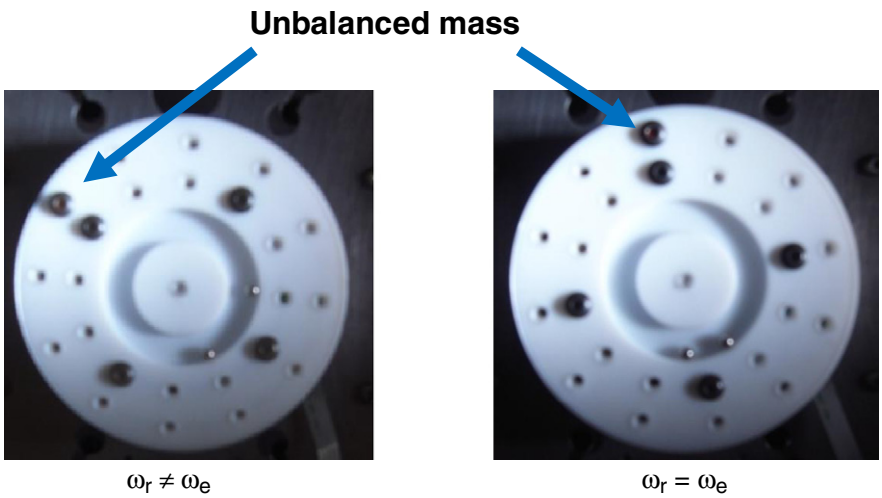

Fig. 11. Influence of the external forcing frequency on ball positioning ($F_0 = 15$ N).

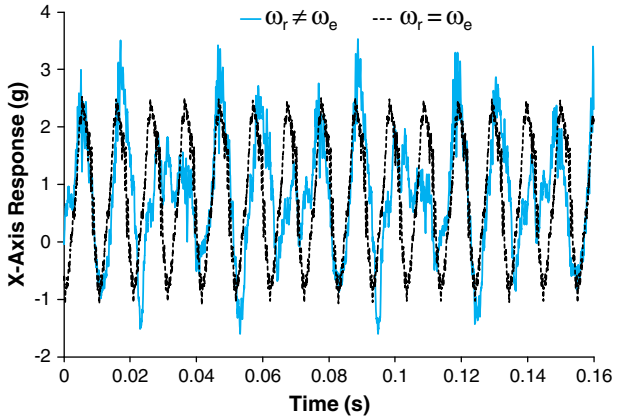

Fig. 12. X-axis responses with external forcing frequencies ($\omega_r = 97$ Hz, $\omega_e = 70$ Hz) and ($\omega_r = \omega_e = 97$ Hz).

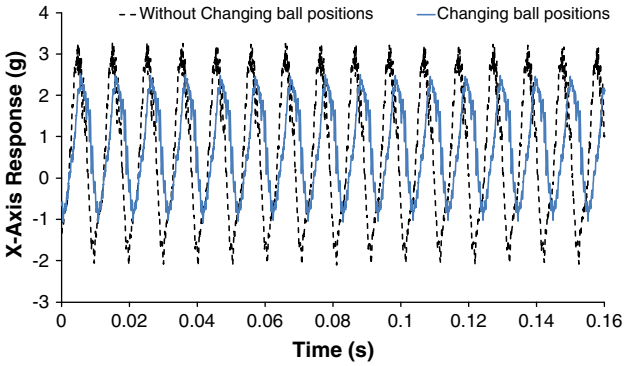

Fig. 13. X-axis residual vibration for $\omega_r = \omega_e$.

The experimental results of the X-axis residual vibration of the rotor system with various external forcing frequencies are shown in Fig. 12. It illustrates that the balancing balls of the ABB can counterbalance the external force to result in smaller residual vibration when $\omega_r = \omega_e$ by changing the ball positions. In essence, the influence of external force on an ABB is similar to that of unbalance. However, it is observed from the experimental results shown in Fig. 13 that the balls may not be displaced because the excessive rolling resistance between the ball and the runway during high operation speed prevents the balls from moving. This situation exists frequently when the external force is applied after the ball has been settled into its steady-state position because of a lack of driving force on balls. This may further deteriorate the balancing performance and cause larger undesired residual vibrations.

5. Conclusions

This study explored how the magnitude, the frequency and even the phase of an external excitation affected ball positioning. The equations governing the motions of the rotor system and the balancing balls were first derived using the Lagrange method and the technique of asymptotic multiple scale analysis. Then, simulations were performed to predict the ball positions under various external forces. Finally, an experimental rig was constructed by using a shaker to apply various excitations to the rotor system. The results indicate that the positions of the balls are not affected when the external forcing frequency is not equal to rotational frequency ($\omega_r \neq \omega_e$). On the other hand, the ball positions are changed by the external force when its frequency is equal to the rotational frequency ($\omega_r = \omega_e$). Therefore, the force acting on the balls as well as the residual vibration becomes larger at the condition of $\omega_r \neq \omega_e$. Moreover, it was also observed from the experiment that the ball would not be displaced because the excessive rolling resistance between the ball and the runway prevented the ball from moving. This phenomenon occurs frequently when the external force is applied after the ball had been positioned. This may further deteriorate the balancing performance and cause larger undesired residual vibrations.

Acknowledgements

The authors are greatly indebted to the National Science Council of the R.O.C. for supporting the research through the following two grants: 97-2221-E-007-050-MY3 and NSC-96-2221-E-007-075.

References

[1] E.L. Thearle, Automatic dynamic balancers part 2—Ring, Pendulum, Ball balancers, Machine Design 22 (1950) 103–106.
[2] T. Majewski, Position errors occurrence in self balancers used on rigid rotors of rotating machinery, Mechanism and Machine Theory 23 (1) (1988) 71–78.
[3] W.Y. Huang, C.P. Chao, J.R. Kang, C.K. Sung, The application of ball-type balancers for radial vibration reduction of high-speed optic disk drives, Journal of Sound and Vibration 250 (3) (2002) 415–430.
[4] C.P. Chao, Y.D. Huang, C.K. Sung, Non-planar dynamic modelling for the optical disk drive spindles equipped with an automatic balancer, Mechanism and Machine Theory 38 (2003) 1289–1305.
[5] C.P. Chao, C.K. Sung, C.C. Wang, Dynamic analysis of the optical disk drives equipped with an automatic ball balancer with consideration of torsional motion, Journal of Applied Mechanics, Transactions of the ASME 72 (6) (2005) 826–842.
[6] R. Horvath, G.T. Flowers, J. Fausz, Influence of nonidealities on the performance of a self-balancing rotor system, Proceedings of IMECE20052005 ASME International Mechanical Engineering Congress and Exposition November 5–11 (2005) Orlando, Florida USA, 2005.
[7] H.A. DeSmidt, Imbalance vibration suppression of a supercritical shaft via an automatic balancing device, Transactions of the ASME Journal of Vibration and Acoustics 131 (041001) (2009) 1–13.
[8] J. Liu, Y. Ishida, Vibration suppression of rotating machinery utilizing an automatic ball balancer and discontinuous spring characteristics, Transactions of the ASME Journal of Vibration and Acoustics 131 (041004) (2009) 1–7.
[9] J. Ehyaei, M.M. Moghaddam, Dynamic response and stability analysis of an unbalanced flexible rotating shaft equipped with n automatic ball-balancers, Journal of Sound and Vibration 321 (3–5) (2009) 554–571.
[10] K. Green, A.R. Champneys, N.J. Lieven, Bifurcation analysis of an automatic dynamic balancing mechanism for eccentric rotors, Journal of Sound and Vibration 291 (2006) 861–881.
[11] D.J. Rodrigues, A.R. Champneys, M.I. Friswell, R.E. Wilson, Two-plane automatic balancing: a symmetry breaking analysis, International Journal of Non-Linear Mechanics 46 (2011) 1139–1154.
[12] T.C. Chan, C.K. Sung, C.P. Chao, Non-linear suspension of an automatic ball balancer, International Journal of Non-Linear Mechanics 46 (2011) 415–424.
[13] C.J. Lu, M.C. Wang, Stability analysis of a ball–rod–spring automatic balancer, International Journal of Mechanical Sciences 53 (2011) 846–854.
[14] Y. Quangang, E.H. Ong, J. Sun, G. Guo, S.P. Lim, Study on the influence of friction in an automatic ball balancing system, Journal of Sound and Vibration 285 (2004) 73–99.
[15] T.C. Chan, C.K. Sung, C.P. Chao, Friction effect on ball positioning of an automatic balancer in optical disk drives, Microsystem Technologies 18 (2012) 1343–1351.
[16] N.V.D. Wouw, M.N.V.D. Heuvel, H. Nijmeijer, J.A.V. Rooij, Performance of an automatic ball balancer with dry friction, International Journal of Bifurcation and Chaos in Applied Sciences and Engineering 15 (1) (2005) 65–82.
[17] R. Horvath, G.T. Flowers, J. Fausz, Passive balancing for rotor system using pendulum balancers, Proceedings of the 20th ASME International Biennial Conference on Mechanical Vibration and Noise, Held in Long Beach, California, September 25–28, 2005, 2005.